RPE | Radiation Physics & Engineering
A Peer-Reviewed Journal
Published by K.N. Toosi University of Technology
http://rpe.kntu.ac.ir
Research Article

Radiation Physics and Engineering 2023; 4(3):53–64

Investigation of key phenomena in increasing the fusion energy gain of neutron-free fuel

Roohalah Mirzaeian, Seyedeh Nasrin Hosseinimotlagh*, Mahboobeh Shaghaghian

Department of Physics, Shiraz Branch, Islamic Azad University, Shiraz, Iran

HIGHLIGHTS

- We used as the role of avalanche kinetics of protons effects on the increasing of amount of energy gain for $p^{11}B$ fuel.
- The effects of bremsstrahlung radiation and ion and electron energy exchange rate have been evaluated.
- The temperature of the electron is kept lower than that of the ion, which improves fuel performance
- The number of alpha particles obtained coincides with the latest research and leads to an enhancement of about 13%.

ABSTRACT

In recent years, various designs for controlled thermonuclear fusion based on the $p^{11}B$ reaction have been reviewed and optimized. In this article, to achieve more energy gain for $p^{11}B$ neutron-free fusion reaction, we used as newer cross-section formula and entered two key phenomena: a) avalanche and b) kinetics of protons. Then, the effects of bremsstrahlung radiation and ion and electron energy exchange rate have been evaluated by introducing relativistic effects and its role on improving fusion energy gain. As a result, the temperature of the electron is kept lower than that of the ion, which improves fuel performance. Finally, it leads to an increase in the number of protons at higher energies compared to the pure Maxwellian distribution and it causes a significant increase in reactivity compared to previous research. Also, the number of alpha particles obtained through calculations coincides with the latest research and leads to an enhancement of approximately 13%. This means that by improving the fusion cross-section of $p^{11}B$, our calculations show that considering the avalanche effects, the range of achievable energy gain in the temperature range of 300 to 500 keV and the stable characteristic time of 0.64 ps reaches 89 to 111. While in the same temperature range and with the stable characteristic time of 0.74 ps, regard free of the cross-section, the energy gain range is 75 to 98.

KEYWORDS

Avalanche
Cross-section
Gain
Kinetic model
Temperature

HISTORY

Received: 18 February 2023
Revised: 10 April 2023
Accepted: 1 May 2023
Published: Summer 2023

1 Introduction

Carbon dioxide diffusion in the air was tolerable until 1960 without climate change. Since then, carbon dioxide diffusion has increased almost five times. And it is expected to two times again in the future years. As you can see, climate change is evident by increasing the average temperature, due to the effect of greenhouse gases, with the rapid rise of the ocean level due to the melting of the glaciers. On the other hand, mankind's need to produce electricity with the very high costs of building power plants led mankind to go for low-carbon energy, such as nuclear energy, which produces energy about 10 million times more than a chemical reaction. In the discussion of nuclear energy, nuclear fusion is one of the most promising and impressive paths in the search for new sources of energy for various reasons, including unlimited fuel resources. Meanwhile, fusion systems with $p^{11}B$ fuel have significant advantages over systems based on D-T or D-D fuels. Because radioactive tritium and energetic neutrons are not produced in it. This is a clean reaction, and the energy released from this reaction is the kinetic energy of alpha particles instead of neutrons:

$$^{11}B + p \rightarrow 3\alpha + 8.7\ \text{MeV} \quad (1)$$

The $^{11}B(p,\alpha)\alpha\alpha$ reaction at incident proton energies $E_p < 4$ MeV has been studied since the 1930s (Hora et al., 2021; Labaune et al., 2013; Martinez-Val et al., 1996; Moreau, 1977; Levush and Cuperman, 1982). In such a plan, the interaction between B-11 nucleus and

*Corresponding author: hosseinimotlagh@iaushiraz.ac.ir

https://doi.org/10.22034/rpe.2023.386226.1118
https://dorl.net/dor/20.1001.1.26456397.2023.4.3.7.5

the incident proton takes place, and as a result, three alpha particles are produced. In addition, the production of characteristic 718 keV gamma rays will follow (Ishikawa et al., 2004; Sikora and Weller, 2016a). It should be noted that the proton-boron nuclear fusion reaction using B-11 nuclei does not produce instantaneous gamma rays. In which, when the proton-boron nuclear fusion reaction occurs, first the B11 nucleus in an excited state converts to a carbon nucleus (C*-12), then this exciting carbon nucleus may split into an alpha particle with an energy of 3.76 MeV and a beryllium nucleus (Be-8). After that, this beryllium nucleus decays into two alpha particles with an energy of 2.74 MeV. In general, three alpha particles are emitted at the site of the proton-boron nuclear fusion reaction. These processes can be represented by the equations: a) $^{11}B + p \rightarrow {}^{12}C^*$, b) $^{12}C^* \rightarrow {}^{8}B + \alpha$ (3.76 MeV), c) $^{8}Be \rightarrow 2\alpha$ (2.74 MeV). Besides these reactions, the alpha-proton-alpha avalanche reaction is also investigated. Because based on these types of reactions, they provide an unexpected increase in the production of alpha particles. This reaction starts from the collision of an alpha particle with a proton which is at rest. This process accelerates the proton to a high enough energy that it can be captured by one B-11. This capture reaction produces three alpha particles that have enough energy to re-accelerate a stationary proton, making it possible to create an avalanche effect (Eliezer et al., 2016; Hora et al., 2015).

Proton-boron nuclear fusion reaction proceeds through a two-step process involving the emission of a primary α-particle followed by two secondary α-particles emitted from the decay of Be-8. Therefore, based on the cross-section data collected, this reaction can be described through its behavior in resonances $E_p = 0.675$ MeV and $E_p = 2.64$ MeV. At $E_p = 0.675$ MeV, primary particles are formed from the decay of the 2^- state in C*-12 which has $l = 3$, and the first excited 2^+ state, Be-8 constitutes. Then Be-8 decays into two particles with $l' = 2$. The 3^- state of C*-12, in which $E_p = 2.64$ MeV is formed, has two possible decay states. Primary alpha particles can be emitted with $l' = 1$ to the first excited state Be-8 or with $l = 3$ to the ground state 0^+. The remaining nucleus (Be-8) then decays and emits two secondary α particles.

However, the reactivity of the p^{11}B nuclear fusion reaction is very low in thermal equilibrium to compete with radiation losses due to the large Coulomb barrier between them and the low fusion cross-section compared to D-T. Therefore, ignition conditions are not achieved in this reaction (Magee et al., 2023). Therefore, in these years, to solve this problem, various plans have been made to perform controlled thermonuclear fusion based on the p^{11}B nuclear fusion reaction (Hora et al., 2021), and the reactivity of p^{11}B fusion plasma has been reviewed at different times.

But the main problem that appears here is related to the high temperature of the ion, which requires high reactivity to reach this temperature. When the temperature rises, the electrons become very hot and lead to intense bremsstrahlung radiation. In such a way many researchers believed that bremsstrahlung radiation prevented the p^{11}B ignition. Since then, many efforts have been made to re-evaluate the reaction cross-section data, which changes the reactivity of p^{11}B by about 20%, which occurs in the temperature range of 300 to 500 keV. Furthermore, we must keep in mind that the proton distribution function may deviate from Maxwellian in the energy range that has the main reactivity contribution. Therefore, we must calculate the fusion energy using the proton distribution resulting from solving the kinetic equation. In this research, our main goal is to optimize the neutron-free p^{11}B fusion reaction power by improving the cross-section and taking into account the correct orbital motion of the primary alpha particle and kinetic effects. Under these conditions, the number of protons increases at higher energies

compared to the pure Maxwellian distribution function. Because in this case, the kinetic effects of proton scattering on non-thermal alpha particles as well as the lowering of the number of protons with higher energy by colder electrons have been taken into account. To achieve more reactivity in free time and achieve higher fusion gain, we organize this paper as follows. In the second part, we examine the changes of the differential cross-section, $\mathrm{d}\sigma/\mathrm{d}\Omega$, in terms of the scattering angle , and from that, we determine the total cross-section and the fusion reactivity of p^{11}B, respectively.

After that, in the third part, we present the optimal fusion power of the desired reaction, taking into account the kinetic effects on the proton distribution function. In the fourth part, the effects of bremsstrahlung radiation and ion and electron energy exchange rates are calculated and studied by introducing relativistic effects and their role in improving the fusion energy gain related to the p^{11}B reaction. After that, in the fifth part, we will write the point kinetic equations governing the p^{11}B fusion reaction, taking into account the mechanism of the avalanche reactions of producing alpha particles. We solve them under the existing conditions as a function of temperature and time for the old and upgraded cross-sections. And finally, we conclude.

2 Evaluation of the differential cross-section and enhanced reactivity of p^{11}B fusion

As explained in the first part, the high temperature causes the electrons to heat a lot and finally creates strong bremsstrahlung radiation and prevents the ignition of p^{11}B. Also, the progress in precision instruments along with the correct identification of the size of the orbital motion of the primary alpha particle as $l = 3$ leads to a re-evaluation and ultimately change of cross-section data (Stave et al., 2011; Wurzel and Hsu, 2022; Buxton et al., 2019). Accordingly, a suitable expansion to obtain the differential cross-section in terms of Legendre polynomials is according to the following relation (Sikora and Weller, 2016b):

$$\frac{\mathrm{d}\sigma}{\mathrm{d}\Omega} \sum_{i}^{i=i_{Max}} A_i \, P_i(\cos\theta) \qquad (2)$$

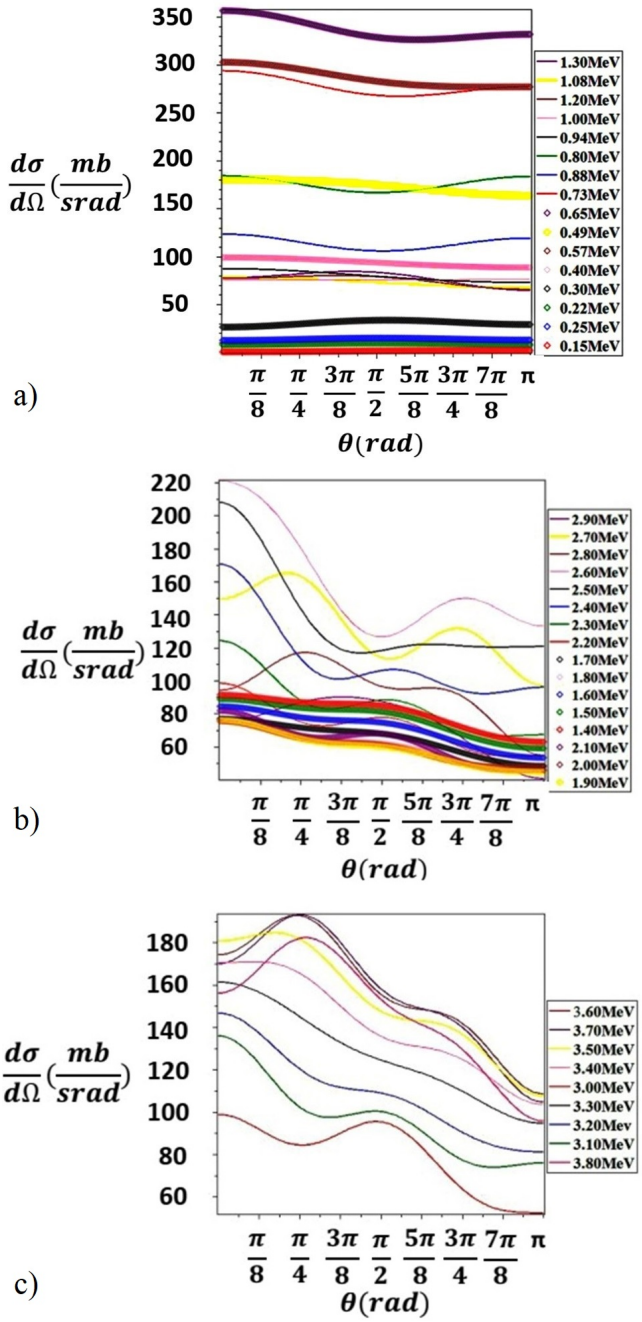

Figure 1: Variations of upgraded d/d in terms of θ for different ranges of proton energies: a) $0.15 < E_p$ (MeV)< 1.3. b) $0.15 < E_p$ (MeV) < 1.3. c) $3.0 < E_p$ (MeV) < 3.8 .

The data obtained for $E_p < 1.4$ MeV, up to the order of expansion $i = 2$, have good accuracy, while for $E_p \geq 1.4$ MeV, they have good accuracy up to the order of expansion $i = 4$. In the graphs of Fig. 1, according to Eq. (2), we show the variations of the differential cross-section $\mathrm{d}\sigma/\mathrm{d}\Omega$ in terms of the scattering angle θ, for different proton energies (E_p).

As can be seen from Fig. 1-a, $\mathrm{d}\sigma/\mathrm{d}\Omega$ variations in terms of θ are different for different proton energies E_p. As the energy increases from $E_p = 0.15$ MeV to $E_p = 0.65$ MeV, the quantity $\mathrm{d}\sigma/\mathrm{d}\Omega$ increases rapidly and has an upward trend, and its peak is observed at $E_p = 0.65$ MeV. $\mathrm{d}\sigma/\mathrm{d}\Omega$ decreases with increasing E_p in the range of 0.65 to 1.3 MeV. Meanwhile, in the energy range of $0.15 < E_p$ (MeV) < 1.3, the obtained numerical values of $\mathrm{d}\sigma/\mathrm{d}\Omega$ do not fluctuate much compared to θ. By looking at Fig. 1-b, it can be seen that $\mathrm{d}\sigma/\mathrm{d}\Omega$ has a downward and upward trend with increasing Ep until two peaks are observed at proton input energies $E_p = 1.4$ MeV and $E_p = 2.6$ MeV. And according to Fig. 1-c, another peak is observed at $E_p = 3.7$ MeV. But as these graphs show, the biggest peak and the most changes in d/d occur at the energy $E_p = 0.65$ MeV, and in this energy, the changes in $\mathrm{d}\sigma/\mathrm{d}\Omega$ have a downward trend in terms of θ and from 350 mb.srad^{-1} it reaches to an approximate 300 mb.srad^{-1}. Then using the relation:

$$\sigma = \int \mathrm{d}\sigma \frac{\mathrm{d}\sigma}{\mathrm{d}\Omega} \tag{3}$$

we have determined the total upgraded cross-section for $p^{11}B$ and plotted its variations in terms of E_p (see Fig. 2).

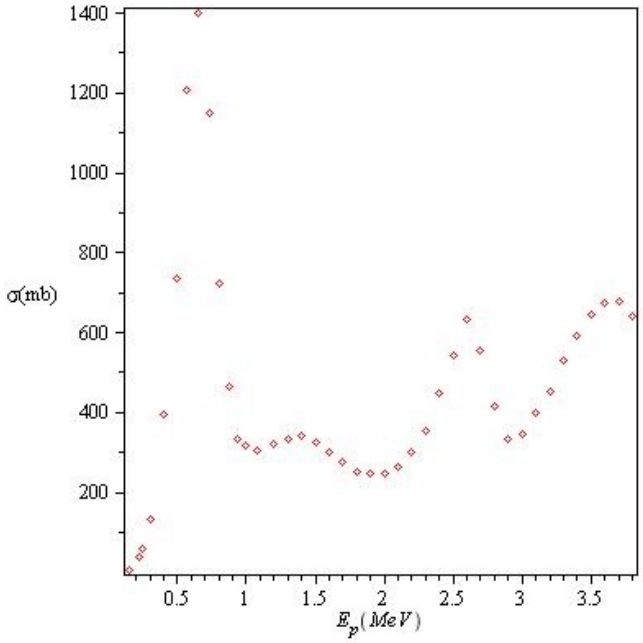

Figure 2: Variations of the total upgraded cross-section for $p^{11}B$ fuel in terms of E_p.

As can be seen from Fig. 2, the total cross-section has four peaks in the proton energy range of $150 \leq Ep$ (keV) ≤ 380. With increasing energy from $E_p = 0.15$ MeV to $E_p = 0.65$ MeV, σ has a rapid upward trend and its peak can be seen at $E_p = 0.65$ MeV. This upward and downward trend continues until other peaks are observed at the proton incident energies $E_p = 1.4$ MeV, $E_p = 2.6$ MeV, and $E_p = 3.7$ MeV. But as these graphs show, the largest peak and the most variations of occur at the energy $E_p = 0.65$ MeV. Reactivity is defined as σv, where σ is the probability of fusion reaction and v is the relative speed of both reactive particles in fusion fuel. We can write the average reactivity for the $p^{11}B$ reaction as follows (Putvinski et al., 2019):

$$\langle \sigma v \rangle = \int f_p(v_p) f_B(v_B) \sigma(u) u \, \mathrm{d}^3 v_P \, \mathrm{d}^3 v_B \tag{4}$$

where $u = |v_p - v_B|$. By substituting the Maxwellian distribution functions $f_p(v_p)$ and $f_B(v_B)$, the above relation is rewritten as follows:

$$\langle \sigma v \rangle = \frac{(8/\pi)^{1/2}}{\mu^{1/2}(k_B T)^{3/2}} \int_0^{\infty} \sigma E \exp(-\frac{E}{k_B T})\, \mathrm{d}E \quad (5)$$

where μ is the reduced mass, k_B is Boltzmann's constant, T is the temperature, σ is the total cross-section of the fusion reaction, v is the relative velocity and E is the energy of the center of mass. Knowing the upgraded σ and using the above formula, we have drawn the variations of average upgraded reactivity in terms of incident proton energy as shown in Fig. 3. As expected and seen from this figure, the reactivity of $p^{11}B$ increases with increasing ion temperature.

From the comparison between the graph obtained in Fig. 3 and the results in older articles, we find that this $p^{11}B$ reactivity is about 20% better than the old reactivity. Instead of this reactivity reaching its current maximum value at temperatures above 600 keV, it reaches this value in the temperature range of 300 to 500 keV.

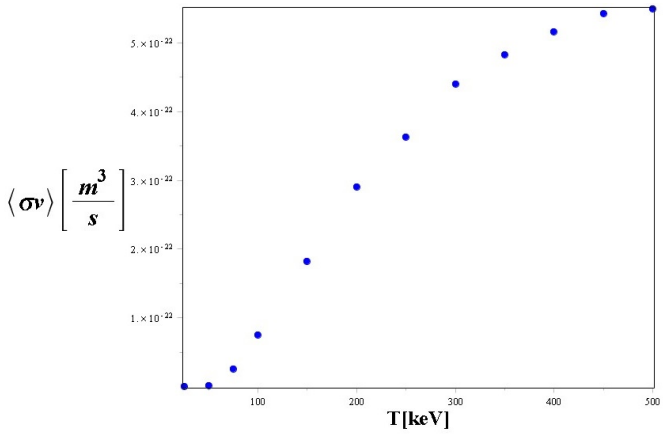

Figure 3: Variations of upgraded reactivity of $p^{11}B$ fuel according to ion temperature T.

3 Optimum estimation of the enhanced fusion power of the $p^{11}B$ reaction by considering the kinetic effects on the proton distribution function

We know that the fusion power density is obtained according to the following relationship (Putvinski et al., 2019):

$$P_{\mathrm{fus}} = n_p n_B \langle \sigma v \rangle Y \quad (6)$$

where n_p and n_B are the proton and boron number density, respectively. Y is the fusion energy and its value for $p^{11}B$ is: $Y = 8.68$ MeV. It should be noted that in this article, fusion alphas are confined enough to transfer the excess energy caused by reactive protons and boron to protons and electrons, and kinetic energy is returned to the plasma and does not affect the overall power balance. Now, to apply kinetic effects, in Eq. 6, we examine these effects on the proton distribution function. In this approximation, the kinetic equation for the proton distribution function is as follows (Putvinski et al., 2019):

$$\frac{1}{v^2}\frac{\partial}{\partial v} v^2 \Big[\frac{F_p}{m_p} f_p + D_p \frac{\partial F_p}{\partial v} \Big] - v_{\mathrm{fus}}(v) f_p + S(v) = 0 \quad (7)$$

In Eq. 7, which is the same kinetic equation related to the proton distribution function, symbols D and F stand for diffusion and dynamic friction, respectively. $S(v)$ is the net source of protons, including fueling and dissipation in the system. $v_{\mathrm{fus}}(v)$, is the rate of proton depletion and loss in fusion reactions. Also, the parameters D_p, F_p, and v_{fus} can be calculated from the following expressions:

$$D_p = D_{pp} + D_{pB} + D_{pe} + D^*_{p\alpha} \quad (8)$$

$$F_p = m_p^2 v \Big(\frac{D_{pp} + D_{pB}}{T} + \frac{D_{pe}}{T_e} \Big) + F^*_{p\alpha} \quad (9)$$

$$v_{\mathrm{fus}}(v) = \int f_B(v_B)\sigma(u)u\, \mathrm{d}^3 v_B = n_B \sigma(v) V \quad (10)$$

In these equations, m_p is the proton mass, v is the speed of thermal protons, T_e is the electron temperature, T is the temperature of slowed-down alphas, and v_B is the speed of outgoing particles. The four parameters D_{pp}, D_{pB}, D_{pe}, and $D_{p\alpha}$ observed in Eq. (8) are obtained from the following relations, respectively (Putvinski et al., 2019):

$$D_{pp} = \frac{4\pi\Lambda e^4}{m_p^3} \frac{T n_p}{v^3 + (\frac{3\sqrt{\pi}}{4}) v_{T_p}^3} \quad (11)$$

$$D_{pB} = \frac{4\pi\Lambda Z_B^2 e^4 T n_B}{A_B m_p^3 v^3} \quad (12)$$

$$D_{pe} = \eta(T_e) \frac{8\sqrt{\pi}\Lambda e^4 n_e}{3 m_p^2} \sqrt{\frac{m_e}{2T_e}} \quad (13)$$

$$D_{p\alpha} = \frac{4\pi\Lambda Z_\alpha^2 e^4 T n_p}{A_\alpha m_p^3 v^3} \frac{1}{v^3 + (\frac{3\sqrt{\pi}}{4}) v_{th,p}^3} \quad (14)$$

In these equations, Λ is the Coulomb logarithm and m_e is the electron mass. Here, a correction factor $\eta(T_e)$ is introduced which is related to relativistic effects in electron distribution functions and electron and ion collision rate. For reference temperature $T_e = 150$ keV, $\eta \approx 1.1$. Z_B and Z_α are boron and alpha atomic numbers, respectively, while the thermal speed of protons is $v_{th,p} = \sqrt{2T/m_p}$. The Coulomb logarithms of proton-proton, proton-electron, and proton-boron are given by the following relations, respectively (Hosseinimotlagh, 2016):

$$\ln\Lambda_{pp} = \frac{\ln\sqrt{\frac{\sqrt{T_p}}{4\pi e^2 n_p}}}{\frac{e^2}{E_p + T_p}} \quad (15)$$

$$\ln\Lambda_{pe} = \frac{\ln\sqrt{\frac{T_e^2 + \varepsilon_f^2}{4\pi e^2 n_e}}}{\sqrt{\Big(\frac{e^2}{m_e(\frac{2T_e}{m_e} + \frac{2E_p}{m_p})}\Big)^2 + \Big(\frac{\hbar}{2m_e\sqrt{\frac{2T_e}{m_e} + \frac{2E_p}{m_p}}}\Big)^2}} \quad (16)$$

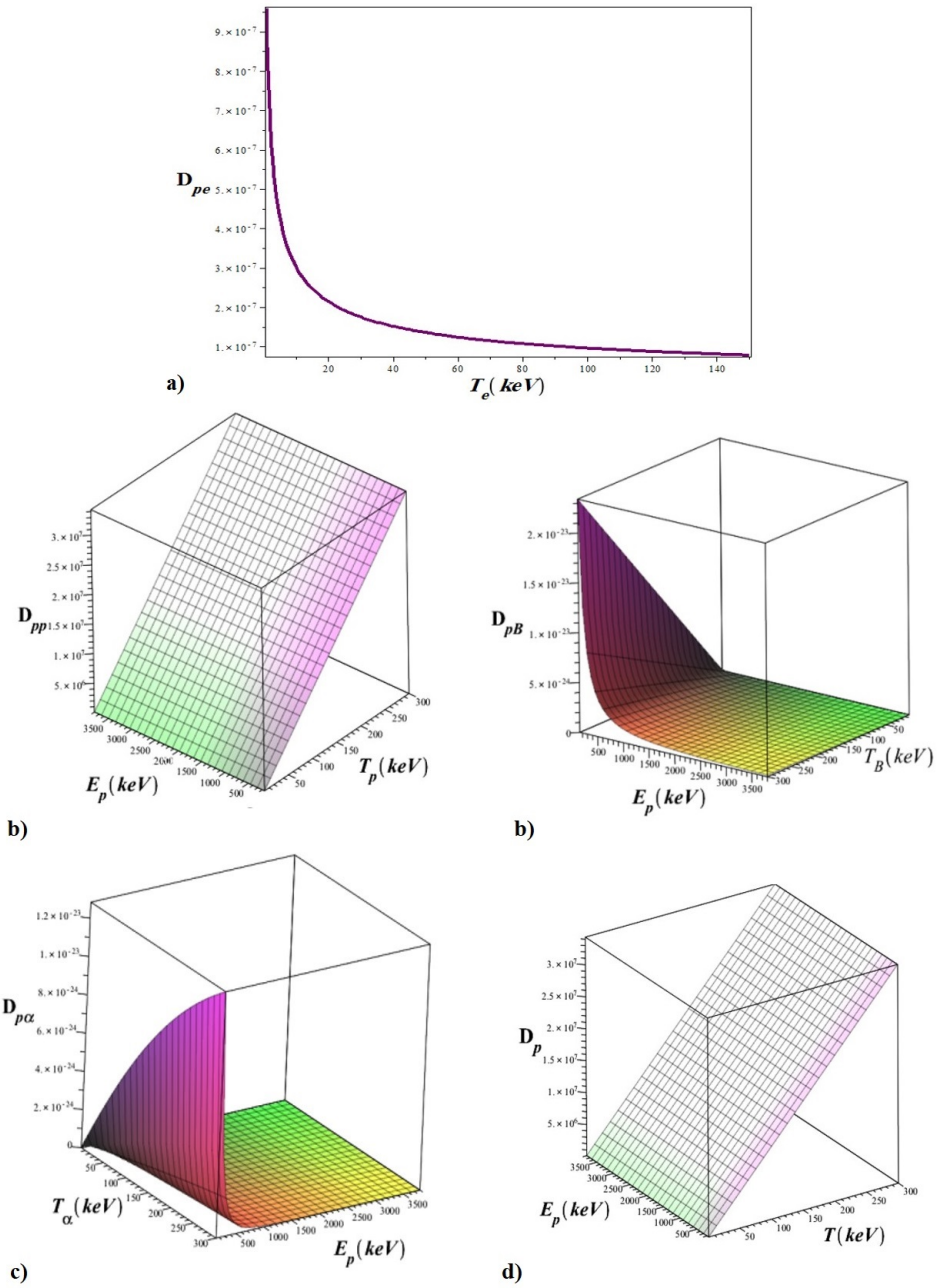

Figure 4: a) 2D variations of D_{pe} versus the temperature. 3-D variations of b) D_{pp}, c) D_{pB}, d) $D_{p\alpha}$, and e) D_p in terms of temperature, and proton energy.

$$\ln\Lambda_{pB} == \frac{\ln\sqrt{\frac{\sqrt{T_B}}{4\pi e^2 n_B}}}{\frac{5e^2}{6E_p + 4T_B}} \tag{17}$$

where $\varepsilon_f = 0.3646(\frac{n_e}{10^{21}\ \mathrm{cm}^{-3}})^{2/3}$ eV. To calculate the numerical values of the parameters mentioned above, we have drawn two-dimensional diagrams of D_{pe} and three-dimensional diagrams of D_{pp}, D_{pB}, $D_{p\alpha}$, and D_p in Fig. 4, respectively.

From the graphs in Fig. 4, it can be seen that for a constant value of E_p, with increasing T, D_{pe} decreases nonlinearly, while D_{pp}, D_{pB}, $D_{p\alpha}$, and finally D_p, which is equal to the sum of these three parameters, are increase linearly, so that the parameter D_p leads to an increase in reactivity. Note that Λ is different in Eqs. (11) to (14) (Sikora and Weller, 2016b). According to the mentioned equations, in Fig. 5 we have drawn the variations of $\ln\Lambda_{pp}$, $\ln\Lambda_{pe}$, and $\ln\Lambda_{pB}$ for different energies E_p.

From examining the graphs drawn in Fig. 5, the following can be seen:

1. $\ln\Lambda_{pB}$, $\ln\Lambda_{pp}$, and $\ln\Lambda_{pe}$ decrease linearly with increasing the proton, boron, and electron numerical density, respectively, for a fixed amount of incident proton energy. Also, if any of these linear densities exceed a certain limit, these reductions take place non-linearly.

2. $\ln\Lambda_{pB}$, for a constant value of incident proton en-

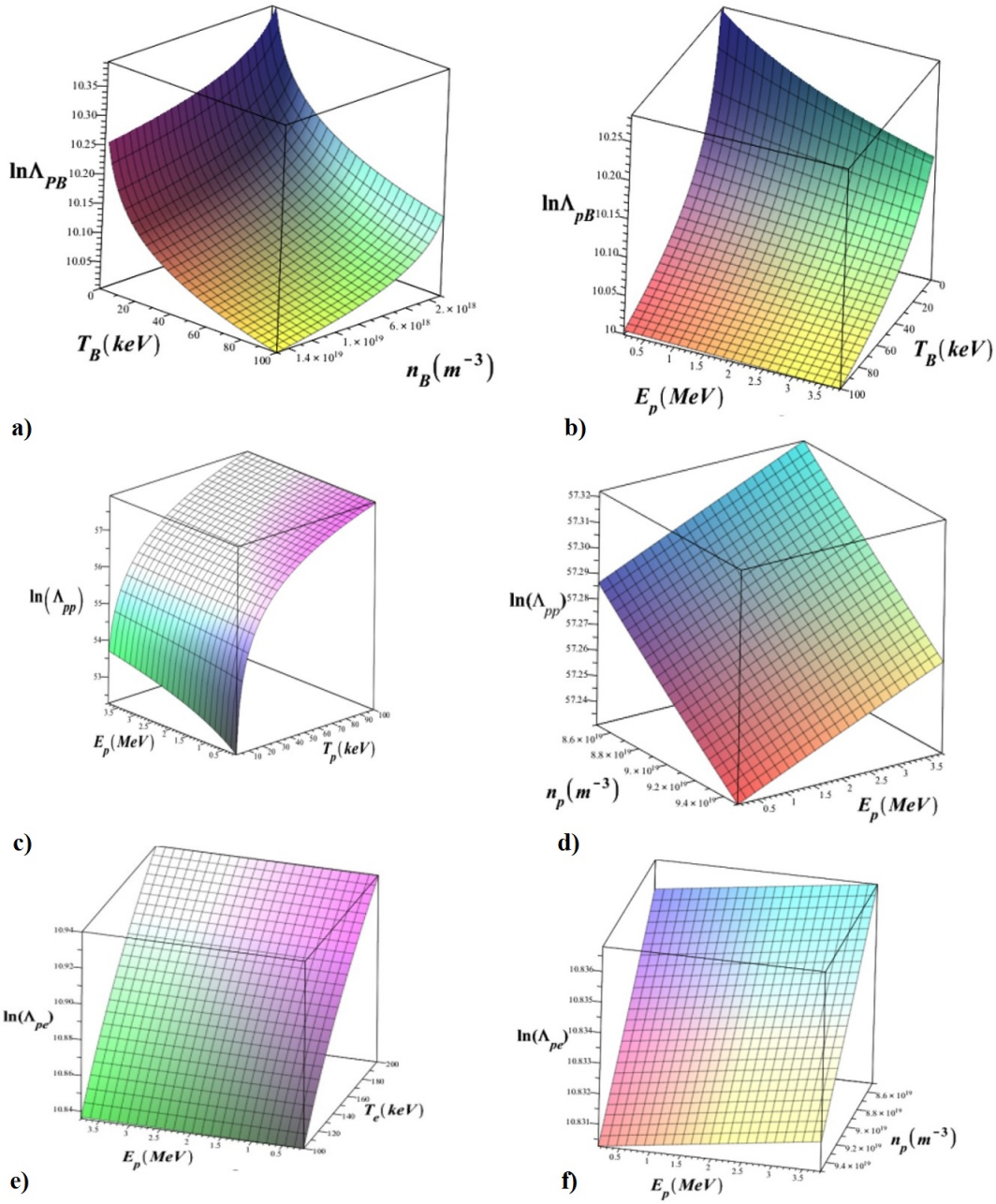

Figure 5: 3-D variations of $\ln\Lambda_{pB}$ in terms of a) T_B and n_B (for $E_p = 0.65$ MeV and $n_p = 0.85 \times 10^{20}$ m^{-3}) b) T_B and E_p. (for $n_e = 10^{20}$ m^{-3} and $n_B = 0.15 \times 10^{20}$ m^{-3}), $\ln\Lambda_{pp}$ in terms of c) T_p and E_p (for $n_p = 0.85 \times 10^{20}$ m^{-3}) d) n_p and E_p (for $T_p = 150$ keV) and $\ln\Lambda_{pe}$ in terms of e) T_e and E_p (for $n_e = 10^{20}$ m^{-3} and $n_p = 0.85 \times 10^{20}$ m^{-3}) f) n_p and E_p (for $n_e = 10^{20}$ m^{-3} and $T_e = 150$ keV)

ergy and boron number density, decreases nonlinearly with increasing boron temperature. While under similar conditions, $\ln\Lambda_{pp}$ increases nonlinearly, and $\ln\Lambda_{pe}$ increases linearly with increasing temperature T_p and T_B, respectively.

3. $\ln\Lambda_{pB}$, $\ln\Lambda_{pp}$, and $\ln\Lambda_{pe}$ decrease linearly with increasing T_p and constant values of temperature and corresponding number density.

Another parameter that plays a very important role in the kinetic equation of the proton distribution function is the amount of proton loss ($v_{\rm fus}(v)$) in the fusion reaction. Therefore, according to Fig. 6, we examine the variations of $v_{\rm fus}(v)$ in terms of incident proton energy and the boron number density.

From Fig. 6-a we see that vfus increases linearly with increasing of n_B for $E_p = 0.65$ MeV and $\sigma = 1400$ mb. While by looking Fig. 6-b, we find that vfus is a coefficient of the cross-section and has similar behavior to it and there are four peaks at the proton energy range of $150 \leq E_p$ (keV) ≤ 380. Except here, the largest peak occurs at $E_p = 3.7$ MeV. In this research, we consider the plasma to be isotropic. It should be noted that according to the Figures and contents mentioned above, the three kinetic effects that are important in estimating the deviation of $f_p(v_p)$ Maxwell distribution and should be considered

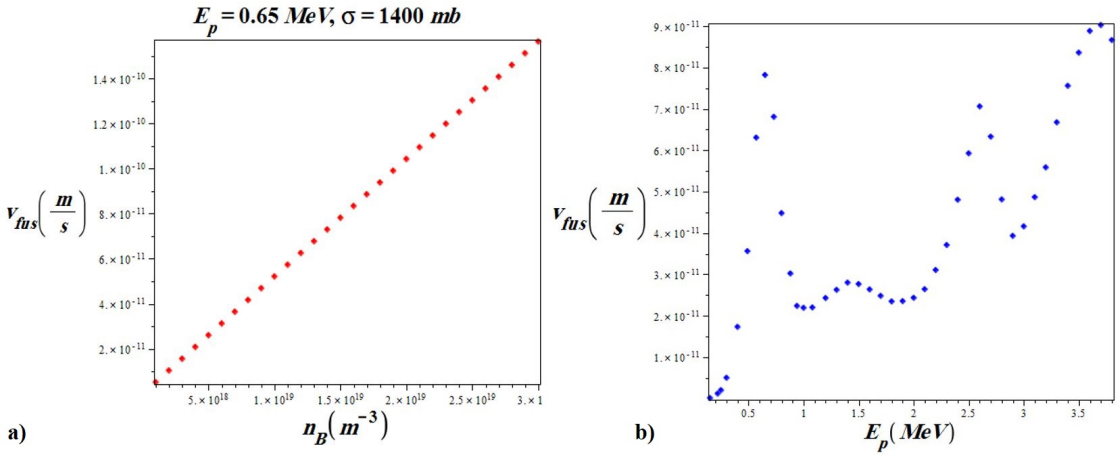

Figure 6: Variations of $v_{\rm fus}(v)$ in terms of a) n_B, and b) E_p.

are as follows:

1. The depletion of the proton energy tail with ablation and proton loss is at the maximum cross-section. This effect leads to a decrease in reactivity.

2. The heating of the proton energy tail is accompanied by the cooling of the cooler electrons. This effect leads to a decrease in reactivity.

3. The heating of the proton energy tail by high-energy alpha particles leads to an increase in the density of the tail, and finally to an increase in reactivity, which according to the above effects, the net effect is positive, and the reactivity increases.

4 The effects of bremsstrahlung radiation and ion and electron energy exchange rate by introducing relativistic effects and its role in the enhancement of $p^{11}B$ fusion energy gain

Around each ion, there is a cover of electrons known as the Debye sheet, which neutralizes the potential caused by the ion outside the Debye shell. When the electron collides with this area and enters the Debye sheath, it is scattered and accelerated under the influence of the electric field in this area. Therefore, we expect to have an energy loss due to bremsstrahlung in plasma environments. Therefore, this is the most important factor that limits the performance of $p^{11}B$ fuel in balanced plasma, which, as mentioned, is created by their collision with ions or with other electrons. The losses due to the escape of particles are improved through the improvement of the confinement system. Studies show that the losses due to the bremsstrahlung radiation of the $p^{11}B$ fusion reaction are more than that of the D^3He. It is not suitable for non-neutral and anisotropic plasma. In conventional reactor designs, with an emphasis on magnetic confinement or inertial confinement, the bremsstrahlung radiation easily escapes from the plasma and is considered a net energy loss. If the plasma could reabsorb this radiation, it would be much more efficient. Therefore, for the density of bremsstrahlung, taking into account relativistic effects, we use Eq. (18) (Putvinski et al., 2019):

$$P_B = 1.62\times10^{-32}\times n_e^2\sqrt{T_e}\Big\{\sum_i \frac{Z_i^2 n_i}{n_e}\times \Big[1+0.7936\frac{T_e}{m_e c^2}+1.874(\frac{T_e}{m_e c^2})^2+\frac{3}{\sqrt{2}}\frac{T_e}{m_e c^2}\Big]\Big\} \tag{18}$$

As seen from Eq. 18, electron bremsstrahlung depends on the product of the number density multiplied by the square of the atomic number of the fuel ions. Now, if the numerical density of boron ions, which has an atomic number of five, is equal to the numerical density of protons, then a major part of the plasma's internal energy is lost through bremsstrahlung radiation. The numerical density of other waste processes is also dependent on the numerical density of boron, and the equimolar of the fuel will increase them significantly. On the other hand, if we reduce the numerical density of boron too much compared to protons, before reaching the desired gain, the boron ions in the target may run out and the fusion will stop.

It should be noted that we can also obtain this bremsstrahlung radiation from the following equation (Putvinski et al., 2019):

$$P_{\alpha,e}+P_{i,e}=P_B \tag{19}$$

where $P_{\alpha,e}$ is electron heating by slowing down alphas, and $P_{i,e}$ is electron heating by thermal protons and boron. We ignore electron energy losses due to synchrotron radiation and conduction energy losses. For more accurate calculations of $P_{\alpha,e}$, we need to consider the additional energy in the source of alpha particles due to the finite kinetic energy of reactive protons and borons. The rate of energy exchange between electrons and thermal ions modified by relativistic effects is (Putvinski et al., 2019; Hosseinimotlagh, 2016):

$$P_{i,e}=7.61\times10^{-28}\times n_e\sum_i \frac{Z_i^2 n_i \ln\Lambda}{\mu_i T_e^{3/2}}\times \Big(1+\frac{m_e}{m_i}\times\frac{T_i}{T_e}\Big)^{-3/2}\Big(1+\frac{0.3T_e}{m_e c^2}\Big)\Big(T_i-T_e\Big) \tag{20}$$

in which relativistic effects are also included. Here $m_i = \mu_i m_p$ gives the mass of the ion in terms of the mass of the proton and the Coulomb logarithm is written as Eq. (21):

$$\ln\Lambda \approx 24 - \ln\left(\frac{\sqrt{n_e}}{T_e}\right) \tag{21}$$

where T_e is the electron temperature in keV and ne is electron density in cm^{-3} (Hay and Fisch, 2015). If there is no other energy loss mechanism for electrons, the least loss related to them is caused by bremsstrahlung radiation. Another important point is the effect of the Coulomb logarithm in fuel, which is very important for reactor designers, and reducing this parameter can improve fuel performance. Because if we calculate the ratio of bremsstrahlung radiation to fusion power, it can be seen that with the reduction of Coulomb's logarithm, P_B/P_f also decreases significantly, which results in better fuel performance. The results of the amount of bremsstrahlung radiation are comparable with the fusion power so that when there are two ion indices p and B with Z_i, then the fusion power density is defined by the following equation (Hay and Fisch, 2015):

$$\begin{aligned} P_{\mathrm{fus}} &= n_p n_B \langle\sigma v\rangle Y \\ &= \frac{\epsilon}{(5\epsilon+1)^2} n_e^2 \langle\sigma v\rangle Y \end{aligned} \tag{22}$$

According to Eq. (22), fusion power is dependent on $\epsilon = n_B/n_p$ and the decrease of ϵ will decrease the energy production through fusion. Therefore, an optimal value must be obtained for the ratio of the number density of boron ions to the number density of protons to maximize the ratio of plasma heating to its cooling. In other words, for a given ion temperature, the upper limit of the electron temperature occurs at a higher temperature. Therefore, in this article, we have used $\epsilon = 0.2$ so that the electron temperature is allowed to increase relatively large. An important point to note is that if is chosen equal to this optimal value at the beginning of the process, due to fuel consumption in fusion reactions, the value of this parameter is reduced and when the fuel temperature rises, it will have a value free than this optimal value. Therefore, the initial value of should be chosen slightly more than this value. Therefore, in Fig. 7, the variations of bremsstrahlung density, the rate of energy exchange between electrons and thermal ions modified by relativistic effects, and the variations of fusion power in terms of temperature and electron density are shown.

Here $m_e c^2$ is the rest energy of the electron, T_e is the electron temperature and ne is the electron number density. It can be seen that from Figs. 7-a, -b and -c, if the electron numerical density is considered constant, with increasing temperature, the energy exchange rate decreases non-linearly, while the bremsstrahlung radiation and fusion power increase non-linearly. Of course, taking into account the correct selection of boron-to-proton density ratio, minimizing the bremsstrahlung power dissipation can result in the acquisition of ion energy at temperatures higher than 100 keV. Also, at a constant electron temperature, with increasing the electron numerical density, the bremsstrahlung radiation increases linearly and the fusion power also increases non-linearly. Now, if we consider the ratio of bremsstrahlung power to fusion power, as the electron temperature increases, this ratio also increases. So to limit the bremsstrahlung radiation, one of the appropriate ways is to reduce the electron temperature, and if the ion and electron temperatures are equal a self-sustaining burn is impossible. So, using the above information, it seems that the Maxwell conditions and the high temperature of the ion compared to the electron will improve the reaction as much as possible

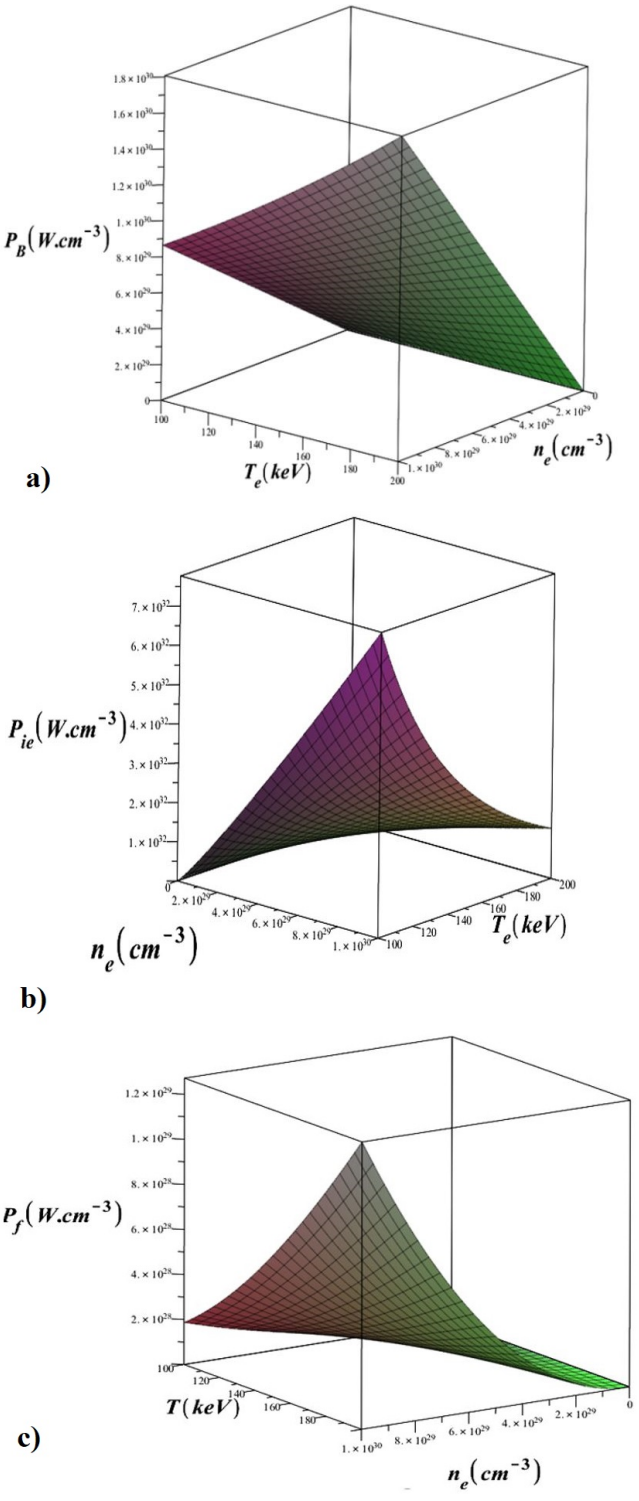

Figure 7: Variations of a) P_B, b) P_{ie}, and c) P_f as a function of T_e and n_e.

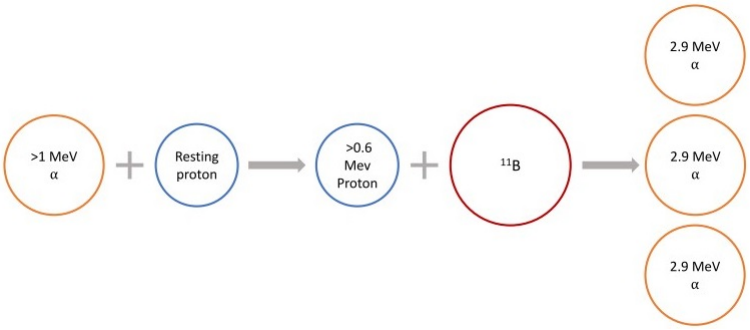

Figure 8: Investigating the alpha-proton-alpha avalanche reaction mechanism. An alpha particle collides with a stationary proton, and as a result, this proton is accelerated to a high enough energy to react with a B-11 and produce three alpha particles.

5 Point kinetic equations governing $p^{11}B$ fusion reaction considering the mechanism of alpha particle generation through avalanche reactions

According to Fig. 8, the mechanisms of the $p^{11}B$ avalanche reaction to produce an avalanche of alpha particles are (Dodder and Gammel, 1952): *i*): An alpha particle created by $p^{11}B$ fusion collides with a proton (which is at rest in the laboratory frame) *ii*): This alpha particle makes a second collision with another proton of the medium (which is at rest). This energetic proton interacts with one B-11 of the environment (which is at rest). *iii*): 3 new alpha particles are created. So that:

$$\begin{aligned} &i)\ p + {}^{11}B \ \rightarrow\ \alpha_1 + \alpha_2 + \alpha_3 \\ &ii)\ \alpha_1 + H(\text{rest.lab}) \ \rightarrow\ \alpha_1' + p' + e \\ &iii)\ p' + {}^{11}B(\text{rest.lab}) \ \rightarrow\ \alpha_1 + \alpha_2 + \alpha_3 + 11e \end{aligned} \tag{23}$$

These three alpha particles can again create accelerated protons and thus create an avalanche of alpha particles. Coupled nonlinear point kinetic equations governing the $p^{11}B$ fusion reaction considering the alpha-proton-alpha avalanche reaction can be written as:

$$\frac{\mathrm{d}n_\alpha}{\mathrm{d}t} = -\frac{n_\alpha}{\tau_\alpha} + 3n_p n_{B-11}\langle\sigma v\rangle \tag{24}$$

$$\frac{\mathrm{d}n_p}{\mathrm{d}t} = -\frac{n_p}{\tau_p} - n_p n_{B-11}\langle\sigma v\rangle + n_p n_\alpha \sigma_{\mathrm{el}} v_\alpha + s_p \tag{25}$$

$$\frac{\mathrm{d}n_{B-11}}{\mathrm{d}t} = -\frac{n_{B-11}}{\tau_{B-11}} - n_p n_{B-11}\langle\sigma v\rangle + s_{B-11} \tag{26}$$

$$\frac{\mathrm{d}E}{\mathrm{d}t} = -\frac{E}{\tau_E} - Q_\alpha n_p n_{B-11}\langle\sigma v\rangle - P_{\mathrm{rad}} + P_{\mathrm{ext}} \tag{27}$$

where σ_{el} is the elastic cross-section, v_α is the relative velocity of proton-alpha before the elastic collision, and P_{rad} is the bremsstrahlung dissipation radiation, which are determined from the following relations:

$$\sigma_{\mathrm{el}}(\alpha, p) \cong \pi\Big(\frac{e^2}{\mu v_\alpha^2}\Big)^2 \tag{28}$$

$$P_{\mathrm{rad}} = A_b Z_{\mathrm{eff}} n_e^2 \sqrt{T} \tag{29}$$

$$n_e = n_p + 5n_{B-11} + 2n_\alpha \tag{30}$$

$$Z_{\mathrm{eff}} = \sum_i \frac{Z_i^2 n_i}{n_e} = \frac{n_p + 25n_{B-11} + 4n_\alpha}{n_e} \tag{31}$$

where $\mu = 4/5m_p$ is the reduced mass of alpha and proton, $v_\alpha = (\frac{2W_\alpha}{m_\alpha})^{1/2}$, and $v_p = (\frac{W_{\mathrm{cm}}p^{11}B\ [\mathrm{keV}]}{4.45\times10^5\ [\mathrm{keV}]})^{1/2}$, where W_α and $W_{\mathrm{cm}}p^{11}B$ are the energy of the produced alpha particle and the energy $p^{11}B$ is the center of mass in the system, respectively.

For $W_\alpha = 1$ MeV, the value of $W_{\mathrm{cm}}p^{11}B = 590$ keV. Also, $A_b = 4.85\times10^{-37}$ W.m^2.keV$^{-1/2}$, $Z_{\mathrm{eff}} = 3$ and $\sigma_{\mathrm{el}} = 10^{-24}$ cm^2 (Dodder and Gammel, 1952; Pusa et al., 2004). By numerically solving coupled non-linear Eqs. (24) to (27), we have determined the time variations of densities n_p, n_{B-11}, n_α, fusion energy production E, and fusion energy gain G at different temperatures for two different states of the old and upgraded cross-sections using Maple programming and the results are shown in Fig. 9.

As can be seen from the graphs in Fig. 9, it can be seen from the comparison of graphs (a and b) as well as (c and d) that temperature variations have little effect on proton and boron number density for both this and old cross-sections. Due to the consumption of fusing fuels, their amount decreases over time and finally reaches the characteristic value of a steady state. By comparing graphs (e and f), (g and h), and (i and j), which are respectively related to the number density of alpha particles, fusion energy, and production fusion gain, it can be seen that all of them have the same behavior with increasing temperature and time. In such a way they first increase with increasing time until they reach their maximum value, then they decrease with increasing time until they reach the characteristic value of the steady state. It should be noted that all these quantities increase with increasing temperature. Also note that in the above calculations, the laser intensity is equal to 3×10^{16} W.cm^{-2} and the initial injection density of protons and borons are considered to be 0.25×10^{20} m^{-3} and 0.15×10^{20} m^{-3}, respectively. To better understand the behavior of the above graphs, pay attention to the numerical values given in Table 1. It can be seen that for the upgraded $\langle\sigma v\rangle$ and certain times given in the table, the maximum densities of alpha particles, fusion energy, and fusion gain are higher than the values of the same quantities for the old $\langle\sigma v\rangle$. Also, with increasing temperature, these maximum values increase. It should be

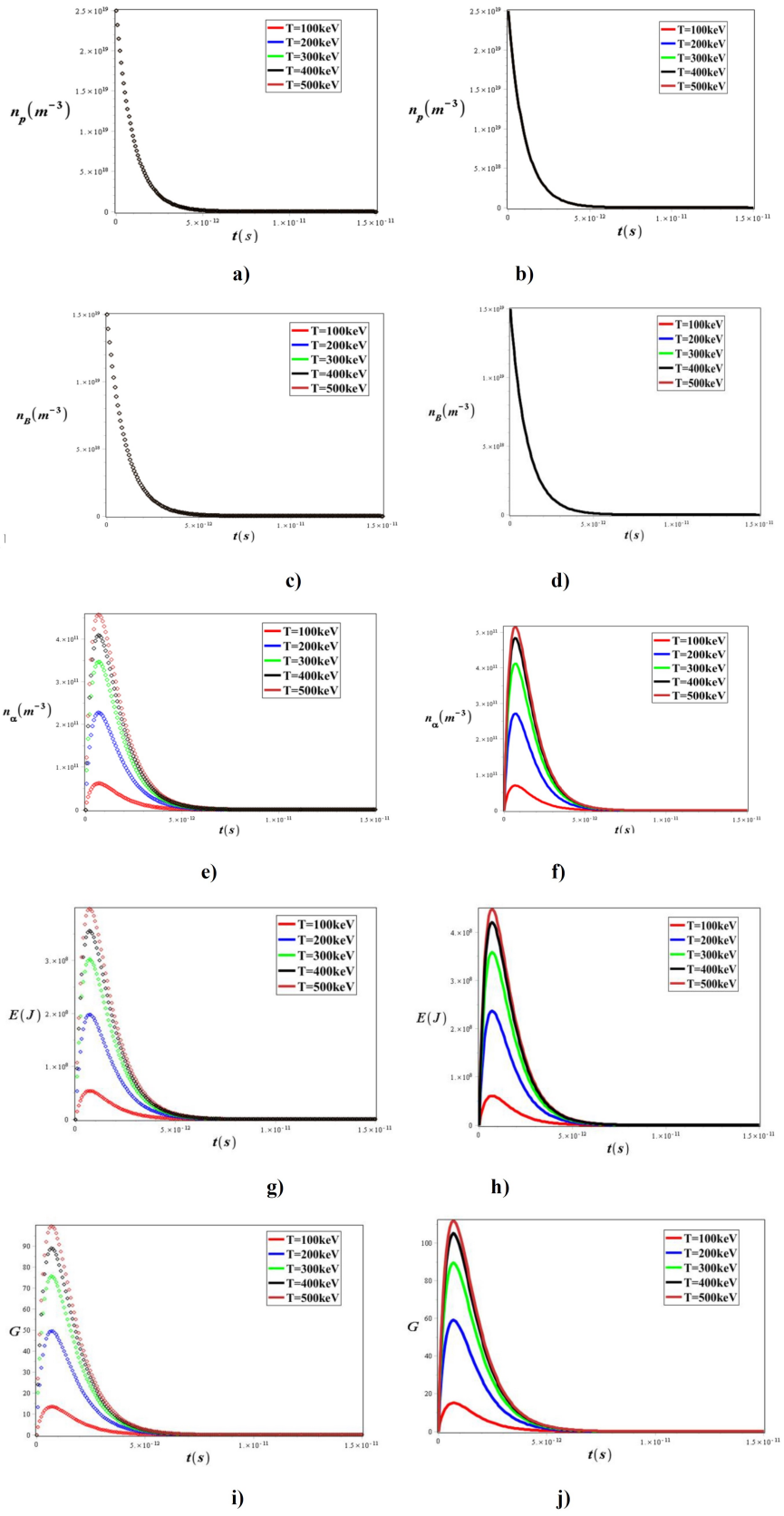

Figure 9: Variations of a) and b) and b) np, c) and d) n_B, e) and f) n_α, g) and h) E, and i) and j) G in terms of time and temperature (notice that right and left graphs correspond to the this cross section and old cross-section, respectively).

noted that at the temperature of 500 keV, the energy gain corresponding to the upgraded $\langle\sigma v\rangle$ is 111 at 0.64 ps and related to the old $\langle\sigma v\rangle$ is 98 at 0.74 ps, which shows an increase in fusion gain of almost 13%.

Table 1: Optimum numerical values of numerical density of alpha particles and fusion energy and fusion gain for two states: *i*) old and *ii*) upgraded reactivity.

T (keV)	i) $\langle\sigma v\rangle$ ($m^3.s^{-1}$) $\times10^{-22}$	ii) $\langle\sigma v\rangle$ ($m^3.s^{-1}$) $\times10^{-22}$	i) n_α (m^{-3}) $\times10^{11}$ $t=0.75\times$ $0.75\times$ s	ii) n_α (m^{-3}) $\times10^{11}$ $t=0.69\times$ 10^{-12} s	i) $E(J)$ $\times10^{8}$ $t=0.78\times$ 10^{-12} s	ii) $E(J)$ ii) $\times10^{8}$ $t=0.62\times$ 10^{-12} s	i) G $t=0.74\times$ 10^{-12} s	ii) G $t=0.64\times$ 10^{-12} s
100	1.14	0.74	0.65	0.75	0.57	0.65	14	17
200	2.78	2.90	2.30	2.70	2.02	2.35	49.8	59
300	3.89	4.40	3.50	4.10	3.05	3.60	75.8	89
400	4.14	5.16	4.10	4.80	3.60	4.20	89.0	105
500	3.98	5.50	4.55	5.12	4.00	4.95	98.5	111

Also, our calculations show that n increases in the upgraded cross-section compared to its value in the old cross-section. In the temperature range of 300 to 500 keV, it changes from 4.1×10^{11} to 5.1×10^{11}, which is in agreement very well with the value obtained from the experiment in (Hora et al., 2021).

In (Hosseinimotlagh et al., 2014), the energy gain of nuclear fusion for the $p^{11}B$ reaction has been calculated without considering the avalanche process and kinetic effects on the proton distribution function and using the following old reactivity equation (Hosseinimotlagh et al., 2014):

$$\langle\sigma v\rangle_{p^{11}B}\ [cm^2.s^{-1}] = C_1\zeta^{-5/6}\xi^2\exp(-3\zeta^{1/3}\xi) + 5.41\times10^{-15}T^{-3/2}\exp(-\frac{148}{T}) \quad (32)$$

here $\zeta = 1 - \dfrac{C_2+C_4T^2+C_6T^3}{1+C_3T+C_5T^2+C_7T^3}$ and $\xi = \dfrac{C_0}{T^{1/3}}$. T is in the range of $50 \le T$ (keV) ≤ 500 and the constant coefficients of C_i are given by: $C_0 = 17.708$ $keV^{1/3}$, $C_1 = 4382\times10^{-16}$ $cm^3.s^{-1}$, $C_2 = -59.357\times10^{-3}$ keV^{-1}, $C_3 = 201.65\times10^{-3}$ keV^{-1}, $C_4 = 1.0404\times10^{-3}$ keV^{-2}, $C_5 = 2.7621\times10^{-3}keV^{-2}$, $C_6 = -0.0091653\times10^{-3}keV^{-3}$, and $C_7 = 0.00098305\times10^{-3}keV^{-3}$. In figure 16 of reference (Hosseinimotlagh et al., 2014), it can be seen that the maximum fusion gain obtained in the temperature range of $50 \le T$ (keV) ≤ 500 is close to 20, while in the present work, the maximum gain for this fusion reaction has been calculated in two cases. Case a) Taking into account the avalanche process, the kinetic effects of the enhanced proton distribution function and the old reactivity formula (Eq. (32)), the fusion energy gain which reaches close to 98 (Fig. 9-i), case b) taking into account the process avalanche process, the kinetic effects of the enhanced proton distribution function and the reactivity value obtained from Eq. (2), which reaches more than 111 (Fig. 9-j). Therefore, this study shows that the consideration of the avalanche process, the kinetics of the proton distribution function and selecting the newer reactivity formula are key parameters in enhancing fusion energy gain.

6 Conclusions

The analysis and re-examination of the basic characteristics of $p^{11}B$ plasma, such as the cross-section of the reaction and the kinetic modification of the proton distribution function, show that $p^{11}B$ fuel can be called one of the best fuels that can be used in the reactor. Because $p^{11}B$ fuel has significant advantages over systems based on D-T or D-D fuels. Because there is no radioactive tritium in it and energetic neutrons are not produced and it is a clean reaction. The energy released from this reaction becomes the kinetic energy of alpha particles and can be used to achieve a higher energy gain. In the kinetic modification of the proton distribution function, according to Eq. (7), various parameters such as D_p and the heating of the proton energy tail play a positive role. In such a way for a constant value of E_p, with increasing T, it increases linearly and causes an increase in reactivity. Also, the heating of the proton energy tail by the energetic alpha particles, followed by increasing in the density of the tail, will increase the reactivity. By examining the ratio of the evaluated fusion power to the bremsstrahlung radiation, taking into account the kinetic corrections, it can be seen that to limit the bremsstrahlung radiation, one of the appropriate ways is to reduce the electron temperature to reduce the effect of dissipation processes that are mainly dependent on the electron temperature. Therefore, the Maxwellian conditions and the high temperature of the ion compared to the electron improve the reaction as much as possible. Our calculations show that taking into account the avalanche effects, temperature variations do not have much effect on proton and boron number density, either with the old or with the upgraded cross-section. And due to the consumption of fusing fuels, their amount decreases over time and finally reaches the characteristic value of a steady state. It can be seen that for the upgraded $\langle\sigma v\rangle$ and certain times given in Table 1, the maximum density of alpha particles, fusion energy, and fusion gain are higher than the values of the same quantities for the old $\langle\sigma v\rangle$. And with increasing temperature, these maximum values increase. Our calculations show that at a temperature of 500keV, the energy gain corresponding to the upgraded $\langle\sigma v\rangle$ is 111 at 0.64 ps and that of the old $\langle\sigma v\rangle$ is 98 at 0.74 ps, which shows an increase in an energy gain of almost 13%. Therefore, this study shows that the consideration of the avalanche process, the kinetics of the proton distribution function and selecting the newer reactivity formula are key parameters in enhancing fusion energy gain.

Acknowledgment

This work is supported by the Islamic Azad University of Shiraz.

Conflict of Interest

The authors declare no potential conflict of interest regarding the publication of this work.

References

Buxton, P., Connor, J., Costley, A., et al. (2019). On the energy confinement time in spherical tokamaks: Implications for the design of pilot plants and fusion reactors. *Plasma Physics and Controlled Fusion*, 61(3):035006.

Dodder, D. and Gammel, J. (1952). Elastic scattering of protons and neutrons by helium. *Physical Review*, 88(3):520.

Eliezer, S., Hora, H., Korn, G., et al. (2016). Avalanche proton-boron fusion based on elastic nuclear collisions. *Physics of Plasmas*, 23(5):050704.

Hay, M. J. and Fisch, N. J. (2015). Ignition threshold for non-Maxwellian plasmas. *Physics of Plasmas*, 22(11):112116.

Hora, H., Eliezer, S., and Nissim, N. (2021). Elimination of secondary neutrons from laser proton-boron fusion. *Laser and Particle Beams*, 2021:1–3.

Hora, H., Korn, G., Giuffrida, L., et al. (2015). Fusion energy using avalanche increased boron reactions for block-ignition by ultrahigh power picosecond laser pulses. *Laser and Particle Beams*, 33(4):607–619.

Hosseinimotlagh, S., Yazdani, M., Jafari, S., et al. (2014). Determination of [rho] R Parameter and Calculation Energy Gain for PB-11 Fusion Reaction. *British Journal of Applied Science & Technology*, 4(31):4420.

Hosseinimotlagh, S. N. (2016). The stopping power of relativistic electrons and laser-accelerated proton beams for fast ignition of D-T and D3He and PB-11 fuels. *International Journal of Hydrogen Energy*, 41(3):1775–1790.

Ishikawa, M., Ono, K., Sakurai, Y., et al. (2004). Development of real-time thermal neutron monitor using boron-loaded plastic scintillator with optical fiber for boron neutron capture therapy. *Applied Radiation and Isotopes*, 61(5):775–779.

Labaune, C., Baccou, C., Depierreux, S., et al. (2013). Fusion reactions initiated by laser-accelerated particle beams in a laser-produced plasma. *Nature Communications*, 4(1):2506.

Levush, B. and Cuperman, S. (1982). On the potentiality of the proton-boron fuel for inertially confined fusion. *Nuclear Fusion*, 22(11):1519.

Magee, R., Ogawa, K., Tajima, T., et al. (2023). First measurements of p11b fusion in a magnetically confined plasma. *Nature Communications*, 14(1):955.

Martinez-Val, J., Eliezer, S., Piera, M., et al. (1996). Fusion burning waves in proton-boron-11 plasmas. *Physics Letters A*, 216(1-5):142–152.

Moreau, D. C. (1977). Potentiality of the proton-boron fuel for controlled thermonuclear fusion. *Nuclear Fusion*, 17(1):13.

Pusa, P., Rauhala, E., Gurbich, A., et al. (2004). Alpha–proton elastic scattering cross sections for ERDA in the resonance region. *Nuclear Instruments and Methods in Physics Research Section B: Beam Interactions with Materials and Atoms*, 222(3-4):686–689.

Putvinski, S., Ryutov, D., and Yushmanov, P. (2019). Fusion reactivity of the pB-11 plasma revisited. *Nuclear Fusion*, 59(7):076018.

Sikora, M. and Weller, H. (2016a). A new evaluation of the ^{11}B(p, α)α α reaction rates. *Journal of Fusion Energy*, 35(3):538–543.

Sikora, M. and Weller, H. (2016b). A new evaluation of the B-11(p, α)α α reaction rates. *Journal of Fusion Energy*, 35(3):538–543.

Stave, S., Ahmed, M., France III, R., et al. (2011). Understanding the B-11(p, α)$\alpha\alpha$ reaction at the 0.675 MeV resonance. *Physics Letters B*, 696(1-2):26–29.

Wurzel, S. E. and Hsu, S. C. (2022). Progress toward fusion energy breakeven and gain as measured against the Lawson criterion. *Physics of Plasmas*, 29(6):062103.

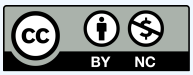

To cite this article:

Mirzaeian, R., HoseiniMotlagh, S. N., & Shaghaghian, M. (2023). The effects of avalanche role on the neutron-less nuclear plasma fusion gain enhancement. *Radiation Physics and Engineering*, 4(3), 53-64.

DOI: 10.22034/rpe.2023.386226.1118

To link to this article: https://doi.org/10.22034/rpe.2023.386226.1118